Nonreciprocal Single-Photon Band Structure

Jiang-Shan Tang,[1,2] Wei Nie,[3,4] Lei Tang,[1] Mingyuan Chen,[1] Xin Su,[1,5] Yanqing Lu,[1,2] Franco Nori,[3,6] and Keyu Xia[1,2,7,8,*]

[1]College of Engineering and Applied Sciences, National Laboratory of Solid State Microstructures, and Collaborative Innovation Center of Advanced Microstructures, Nanjing University, Nanjing 210023, China
[2]School of Physics, Nanjing University, Nanjing 210023, China
[3]RIKEN Quantum Computing Center, RIKEN Cluster for Pioneering Research, Wako-shi, Saitama 351-0198, Japan
[4]Center for Joint Quantum Studies and Department of Physics, School of Science, Tianjin University, Tianjin 300350, China
[5]School of Electronic Science and Engineering, Nanjing University, Nanjing 210023, China
[6]Physics Department, The University of Michigan, Ann Arbor, Michigan 48109-1040, USA
[7]Jiangsu Key Laboratory of Artificial Functional Materials, Nanjing University, Nanjing 210023, China
[8]Key Laboratory of Intelligent Optical Sensing and Manipulation (Nanjing University), Ministry of Education, Nanjing 210023, China

(Received 12 January 2022; accepted 19 April 2022; published 17 May 2022)

We study a single-photon band structure in a one-dimensional coupled-resonator optical waveguide that chirally couples to an array of two-level quantum emitters (QEs). The chiral interaction between the resonator mode and the QE can break the time-reversal symmetry without the magneto-optical effect and an external or synthetic magnetic field. As a result, nonreciprocal single-photon edge states, band gaps, and flat bands appear. By using such a chiral QE coupled-resonator optical waveguide system, including a finite number of unit cells and working in the nonreciprocal band gap, we achieve frequency-multiplexed single-photon circulators with high fidelity and low insertion loss. The chiral QE-light interaction can also protect one-way propagation of single photons against backscattering. Our work opens a new door for studying unconventional photonic band structures without electronic counterparts in condensed matter and exploring its applications in the quantum regime.

DOI: 10.1103/PhysRevLett.128.203602

Introduction.—In analogy to the electronic band structure in condensed matter, a periodic photonic structure exhibits nontrivial band structures and allows defect-immune photon transport [1–4], promising many important applications in light manipulation. Nevertheless, a topological optical system can break time-reversal symmetry and is appealing for backscattering-immune optical isolation only in the presence of an external or synthetic magnetic field, typically causing a considerable loss of photons. Thus, it is highly desirable to achieve one-way photonic band structures, such as nonreciprocal single-photon edge states (SPESs), and band gaps without magnetic fields, in particular, in the *quantum* regime.

Optical nonreciprocity plays an indispensable role in many important applications, including quantum-information processing [5–8], invisible sensing [9], noise-free information processing [10], and unconventional lasing [11]. Conventional nonreciprocal optical devices breaking time-reversal symmetry rely on the weak magneto-optical effect and are incompatible with the integration of periodic photonic microstructures due to the constraint of a strong magnetic field.

Various theoretical schemes and experimental methods have been reported to circumvent the severe constraint of magnetic fields, including optical nonlinearity [12–19], optomechanical resonators [20–22], spinning resonators [23,24], tempospatial modulation of the medium [25–27], or chiral quantum optics systems [28–36].

In contrast to classical methods, a chiral quantum optics system is of special interest because it can realize optical nonreciprocity in the quantum regime [14–16,29–31,33,34] and provides unprecedented capabilities for unconventional quantum information processing [37–40]. The chiral interaction of some QEs with few resonators has been extensively studied and promises important applications [41,42]. The coupled-resonator optical waveguide (CROW) can be used to engineer photonic band structures and thus has been widely investigated [43–47]. Photonic band structures with chiral interaction between QEs and a resonator array are attracting growing interest [48–50]. Nevertheless, magnetic-free nonreciprocity in such systems has barely been addressed.

By exploring the chiral interaction between an array of QEs and a 1D CROW, here we show that nonreciprocal single-photon band structures, including SPES, band gap, and flat band, can be achieved without a magnetic field. Interestingly, such a chiral QE-CROW system, working in the nonreciprocal band gap, allows frequency-multiplexed and backscattering-immune single-photon circulators. Such magnetic-free photonic behavior reveals essentially

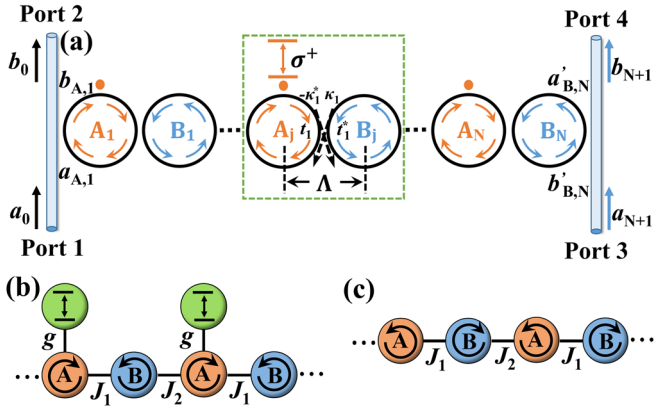

FIG. 1. (a) Schematic of a chiral QE-CROW system containing N unit cells and the input and output waveguides. The arrows represent the circulating direction of the whispering-gallery mode for an input to port 1 or 3 (forward input). The photon incident to ports 2 and 4 (backward input) excites the oppositely propagating resonator modes. The QEs with σ^+-polarized optical transitions are periodically coupled to the clockwise resonator mode of the sublattice A in each unit cell; see dashed box. (b) The L-shaped trimer chain in the forward-input case. (c) The dimer chain for the backward-input case.

different physics from its electronic counterpart in condensed matter.

System and model.—The schematic of the chiral QE-CROW system is depicted in Fig. 1. In the CROW, the evanescent field of each microring resonator is almost perfectly circularly polarized and thus possesses nearly unitary optical chirality [29,30,36], i.e., possesses spin-momentum locking [51–53]. In each unit cell, the adjacent resonators are separated by Λ and coherently coupled via evanescent fields. Each resonator supports two degenerate optical whispering-gallery modes circulating along either the clockwise (CW) or counterclockwise (CCW) direction. We divide the resonators into A and B sublattice groups, respectively denoted as R_A and R_B. In each unit cell, a two-level QE with frequency ω_q is only embedded in the A-sublattice resonator R_A, but decouples from the B-sublattice resonator R_B. Within a cell, the CW (CCW) mode of R_A couples to the CCW (CW) mode of R_B with strength J_1; see the green box in Fig. 1(a). The jth resonator R_A couples to the $(j+1)$th resonator R_B in the next cell with strength J_2. The oppositely circulating whispering-gallery modes in the sublattices A and B form N unit cells with a lattice constant of 2Λ [44]. We assume that the resonators, with resonance frequency Ω and internal dissipation rate γ_{in}, are identical.

Hereafter, we consider only a single excitation in the QE-CROW system. The QEs can be precisely positioned atoms [30,45,54], quantum dots [42,55,56], valley-selective excitons [36,57,58], or nanopillars covered by monolayers [59,60]. By optically initializing the QEs in specific spin ground states or shifting the transition energy with a circularly polarized field via the optical Stark effect, we can induce a chiral transition in the QE. Without loss of generality, we assume that the QE transition and the evanescent field of the CW mode of R_A are both σ_+-polarized. Thus, we create a chiral interaction between the QE and the CW mode of R_A without using a magnetic field [28–31,34–36]. However, the QE decouples from the CCW mode [29–31,36].

When a single photon is incident into port 1 or 3, namely the forward-input case, the CW modes in the R_A resonators and the CCW ones in the R_B resonators are driven. We refer to this excitation as the $CW_A - CCW_B$ supermode (opposite to the $CCW_A - CW_B$ supermode). In this case, the QEs are coupled to R_A in each unit cell. The QE-CROW system is equivalent to an L-shaped trimer chain with each cell containing three sublattices [61]; see Fig. 1(b). We now take $\omega_q = \Omega$ and can write the Hamiltonian of the system in the rotating frame as $\hat{H}_{CW_A-CCW_B} = \sum_j^N (g\hat{a}_{j,\circlearrowright}^\dagger \hat{\sigma}_j + J_1 \hat{a}_{j,\circlearrowleft}^\dagger \hat{b}_{j,\circlearrowleft} + \text{H.c.}) + \sum_j^{N-1} (J_2 \hat{a}_{j+1,\circlearrowright}^\dagger \hat{b}_{j,\circlearrowleft} + \text{H.c.})$, where $\hat{a}_{j,\circlearrowright}$ ($\hat{b}_{j,\circlearrowleft}$) is the annihilation operator of the CW (CCW) mode of the R_A (R_B) resonator in the jth unit cell, and $\hat{\sigma}_j$ denotes the lowering operator of the jth two-level QE.

Now we study the band structure of an infinite 1D-CROW model in a single-excitation subspace. We assume a periodic boundary condition along the 1D-CROW chain and apply the Fourier transform $\zeta_k = (1/\sqrt{N}\sum_j e^{-ikj}\xi_j)$ with $\xi_j = (\hat{a}_{j,\circlearrowright}, \hat{\sigma}_j, \hat{b}_{j,\circlearrowleft})^T$; thus, $\hat{H}_{CW_A-CCW_B} = \sum_k \zeta_k^\dagger H_{CW_A-CCW_B}(k)\zeta_k$. Then, in wave vector space, we have

$$H_{CW_A-CCW_B}(k) = \begin{pmatrix} 0 & g & J_1 + J_2 e^{-ik} \\ g & 0 & 0 \\ J_1 + J_2 e^{ik} & 0 & 0 \end{pmatrix}. \quad (1)$$

By defining a unitary and Hermitian matrix, $\chi = [-1, 0, 0; 0, 1, 0; 0, 0, 1]$, we have $\chi H_{CW_A-CCW_B}\chi^{-1} = -H_{CW_A-CCW_B}$. Thus, the system possesses chiral symmetry.

In comparison, if a single photon incidents to port 2 or 4 corresponding to the backward-input case, then the $CCW_A - CW_B$ supermode is driven in each unit cell and the QEs decouple from all resonators. Our system reduces to a dimer chain corresponding to a standard Su-Schrieffer-Heeger (SSH) model [62,63] [see Fig. 1(c)]:

$$H_{CCW_A-CW_B}(k) = \begin{pmatrix} 0 & J_1 + J_2 e^{-ik} \\ J_1 + J_2 e^{ik} & 0 \end{pmatrix}. \quad (2)$$

The band structures and energy spectra of the system in the $CW_A - CCW_B$ and $CCW_A - CW_B$ supermodes can be found by solving the eigenvalues and eigenstates of Eq. (1) and Eq. (2), respectively. In the case related to the $CW_A - CCW_B$ supermode, the QEs interact with the R_A resonators. This interaction causes a phase and amplitude modulation

$e^{i\varphi}$ to the R_A CW mode [64,70]. Here, φ is a complex number. In contrast, the QE-resonator interaction is absent for the $CCW_A - CW_B$ supermode. Thus, the extra modulation disappears, i.e., $\varphi = 0$. The dispersion relations of the $CW_A - CCW_B$ supermode consist of three dispersive bands. It is essentially different from the $CCW_A - CW_B$ supermode, which only contains two bands. Therefore, the single-photon band structures are nonreciprocal in two counterpropagating cases. This nonreciprocal single-photon dispersion occurs because the chiral QE-light coupling breaks the time-reversal symmetry of the system.

A finite 1D-CROW chain with a large number of unit cells can approximately exhibit the property of an infinite chain [44]. Next, we discuss a finite chiral 1D CROW containing N unit cells ($N \geq 1$) and evaluate the single-photon transmission. Two optical waveguides are side-coupled to the terminal resonators as input and output channels. We utilize the transfer matrix method to investigate the transmission properties of the system [46,64]. We consider the forward case. The notations for the field components $\{a\}$ and $\{b\}$ are shown in Fig. 1(a). By successively multiplying the transfer matrices of all the coupling relations, we obtain the transport relation

$$\begin{pmatrix} a_{N+1} \\ b_{N+1} \end{pmatrix} = M \begin{pmatrix} a_0 \\ b_0 \end{pmatrix} \equiv \begin{pmatrix} M_{11} & M_{12} \\ M_{21} & M_{22} \end{pmatrix} \begin{pmatrix} a_0 \\ b_0 \end{pmatrix}, \quad (3)$$

$$M = M_{\text{out}} M_{\text{p,B}} M_{\text{c,1}} M_{\text{p,A}} (M_{\text{c,2}} M_{\text{p,B}} M_{\text{c,1}} M_{\text{p,A}})^{N-1} M_{\text{in}},$$

where

$$M_{\text{p,A}} = \begin{pmatrix} \alpha e^{-i\theta} & 0 \\ 0 & \alpha e^{i(\theta+\varphi)} \end{pmatrix}, \quad M_{\text{p,B}} = \begin{pmatrix} \alpha e^{-i\theta} & 0 \\ 0 & \alpha e^{i\theta} \end{pmatrix},$$
$$M_{\text{c,1}} = \frac{1}{\kappa_1} \begin{pmatrix} 1 & -t_1 \\ t_1^* & -1 \end{pmatrix}, \quad M_{\text{c,2}} = \frac{1}{\kappa_2} \begin{pmatrix} 1 & -t_2 \\ t_2^* & -1 \end{pmatrix},$$
$$M_{\text{in}} = \frac{1}{\kappa_{\text{in}}} \begin{pmatrix} -t_{\text{in}} & 1 \\ -1 & t_{\text{in}}^* \end{pmatrix}, \quad M_{\text{out}} = \frac{1}{\kappa_{\text{out}}} \begin{pmatrix} 1 & -t_{\text{out}} \\ t_{\text{out}}^* & -1 \end{pmatrix}. \quad (4)$$

We define $\{t_{\text{in}}, t_1, t_2, t_{\text{out}}\}$ and $\{\kappa_{\text{in}}, \kappa_1, \kappa_2, \kappa_{\text{out}}\}$ as the transmission and coupling coefficients of the intrasite and intersite resonators, where t_i ($i = \text{in}, 1, 2, \text{out}$) is a real number, κ_i is an imaginary number, and $|t_i|^2 + |\kappa_i|^2 = 1$ [46]. θ indicates the phase change. α is the loss coefficient of propagating single photons and is calculated as $\alpha \approx 1 - 2\gamma_{\text{in}}/\mathcal{F}$ from the intrinsic loss rate γ_{in} of the resonator [70], where $\mathcal{F}$ is the free spectral range of the resonator considered here. The ratio $\kappa_{\text{in}}/\mathcal{F}$ is negligible for our high-quality resonators, yielding $\alpha \approx 1$.

For simplicity, we assume $\kappa_{\text{in}} = \kappa_{\text{out}}$ ($t_{\text{in}} = t_{\text{out}}$). The external losses of the edge resonators A_1 and B_N are $\gamma_{\text{ex}} = \gamma_{\text{ex,1}} = \gamma_{\text{ex,N}} = -\ln(|t_{\text{in}}|) \times \mathcal{F}$. Considering a single-photon entering port 1 ($a_{N+1} = 0$), we obtain the transmission matrix elements between the input and output ports: $T_{12} = |b_0/a_0|^2 = |M_{11}/M_{12}|^2$ and $T_{14} = |b_{N+1}/a_0|^2 = |M_{21} - M_{11}M_{22}/M_{12}|^2$, where T_{mn} is the transmission from port m to port n, with $m, n = 1, 2, 3, 4$. Because the input to port 3 excites the $CW_A - CCW_B$ supermode circulating along the same direction, we have $T_{12} = T_{34}$ and $T_{14} = T_{32}$. When the $CCW_A - CW_B$ supermode is excited in the backward case, the QEs decouple from the resonators and we have $\varphi = 0$. Therefore, we have $T_{mn} \neq T_{nm}$ for $m \neq n$, indicating the occurrence of optical nonreciprocity in our chiral QE-CROW system.

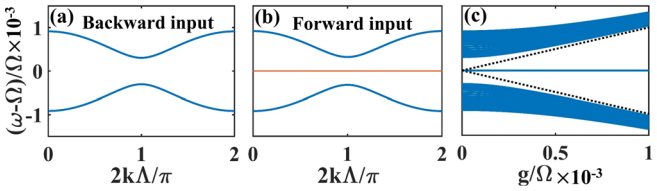

FIG. 2. Single-photon band structures of the chiral QE-CROW system in the case of $J_1 < J_2$. (a) Band structure when the $CCW_A - CW_B$ supermode is excited in the absence of the QEs, i.e., $g/\Omega = 0$. (b) Band structure when the $CW_A - CCW_B$ supermode, coupling to the QEs with $g/\Omega = 10^{-4}$, is driven. (c) Band structures versus the coupling strength g when the $CW_A - CCW_B$ supermode is driven. Other parameters: $J_1/\Omega = 3 \times 10^{-4}$, $J_2 = 2J_1$.

Below, we consider an ideal scenario in which we neglect the QE dissipation by setting the rate $\gamma = 0$.

Nonreciprocal single-photon flat band and edge states.—We first discuss the case $J_1 < J_2$. As seen from the dispersion relations in Fig. 2, the QE-CROW system exhibits a nonreciprocal single-photon band structure. Typically, two dispersive bands of the SSH model appear in the backward case, as shown in Fig. 2(a) [71] for $J_1/\Omega = 3 \times 10^{-4}$ and $J_2 = 2J_1$. The curves with opposite slopes imply two opposite directions of single-photon propagation, corresponding to the input to port 2 or 4 in Fig. 1, respectively. In the forward case, the QEs interact with the R_A resonator. A flat band appears at $\omega = \Omega$ due to the coupling to the QEs, dividing the original band gap into two parts; see Fig. 2(b). Thus, our QE-CROW system allows slow light and delay of single-photon pulses [72–74]. As the QE-resonator coupling strength increases, the two band gaps become wider; see Fig. 2(c).

According to the SSH model, there are left and right SPESs in two opposite-input cases. Unlike the backward case, due to the QE-resonator coupling in the forward case, the left SPES becomes doublet, forming two superstates of the R_A set and the QEs with an energy splitting proportional to the coupling strength g [64]; see the dashed black curves in Fig. 2(c).

We evaluate the Zak phase for the 1D topological invariant, defined as $Z_p = i \int_{-\pi}^{\pi} dk \langle \zeta_{k,p} | \partial_k | \zeta_{k,p} \rangle$, for the pth band ($p = 1, 2, 3$ for the lower, middle, and upper bands). For a small g, a well-defined topological invariant is available. Taking $J_2 = 2J_1$, we have quantized Zak phases,

being $Z_1/\pi = Z_3/\pi = 1$ and $Z_2/\pi = 0$ [64]. As the QE-resonator coupling increases, the effect of g on the bulk bands emerges (in particular, band gaps occur at $J_2 = J_1$). The QE-resonator coupling breaks the inversion symmetry of the SSH model. Thus, the topological invariant is not well-defined and the Zak phase is not quantized [75–78] (see the Supplemental Material [64]).

We also study the effect of Gaussian-distributed on-site disorder. When the standard deviation reaches about $\sigma_{\max}/\Omega = 0.4 \times 10^{-4}$ at $g/\Omega = 10^{-4}$, the SPESs and the flat band are indistinguishable [64]. This means that our system maintains its nonreciprocal SPESs as long as $\sigma_{\max} < 0.4g$, indicating a strong robustness against on-site disorder.

Figure 3 shows energy spectra of a finite unit cell with $N = 20$ and the probability distribution corresponding to the SPESs in the two oppositely circulating supermodes of the system. As for the $\mathrm{CCW_A} - \mathrm{CW_B}$ supermode without coupling to the QEs, there are $2N$ eigenvalues and two degenerate zero-energy SPESs falling in the band gap [see the purple asterisks in Fig. 3(a)]. The wave functions of two edge states localize at the left or right boundary and exponentially decay from the boundaries [see Fig. 3(c)].

In stark contrast, when the system is excited in the $\mathrm{CW_A} - \mathrm{CCW_B}$ supermode, the coupling to the QEs results in N more eigenvalues. The energy spectrum with $N = 20$ and $g/\Omega = 10^{-4}$ is shown in Fig. 3(c). The left SPESs have eigenenergies at $\omega - \Omega = \pm g$ (see the blue asterisks). In Fig. 3(d), the probability of the A sublattice includes the contribution of the QE. Unlike the SPESs of the $\mathrm{CCW_A} - \mathrm{CW_B}$ supermode, the wave functions of these SPESs only localize on the left edge of the system with an exponentially decaying probability distribution at the sites of both the A-sublattice resonator and the QE. The right zero-energy SPES still exists [see the red asterisk in Fig. 3(b)] because the $\mathrm{R_B}$ resonators decouple from the QE. The wave function of this right SPES localizes at the right boundary; see Fig. 3(e). The nonreciprocal SPESs are the unique property of our chiral QE-CROW system. Therefore, for small N, we can realize a single-photon circulator via directional tunneling between the left and right SPESs [64].

Nonreciprocal single-photon band gap.—The case $J_1 > J_2$ opens a band gap but exhibits trivial physical properties. Below we focus on the of interest case $J_1 = J_2$. Figures 4(a) and 4(b) show a nonreciprocal single-photon band gap for oppositely propagating photons. For the backward input, the two bands are closed and thus form continuous conduction bands. In comparison, as in the case of $J_1 < J_2$, the $\mathrm{CW_A} - \mathrm{CCW_B}$ supermode also exhibits two band gaps, separated by a flat band due to the interaction with QEs; see the yellow region in Fig. 4(b). The band gap increases with the QE-resonator coupling strength, permitting a wider nonreciprocal bandwidth. This nonreciprocal single-photon band gap allows to conduct single-photon circulators. The same results can be derived by using the transfer matrix method [64].

The band structures characterize the transmission of single photons. When we consider the 1D CROW with finite unit cells, the conduction band region turns into transmission peaks. We calculate the transmission spectrum of our QE-CROW system with $N = 10$ in the two opposite-propagation cases. For single photons input to port 2 [see Fig. 4(c)], the excited $\mathrm{CCW_A} - \mathrm{CW_B}$ supermode decouples

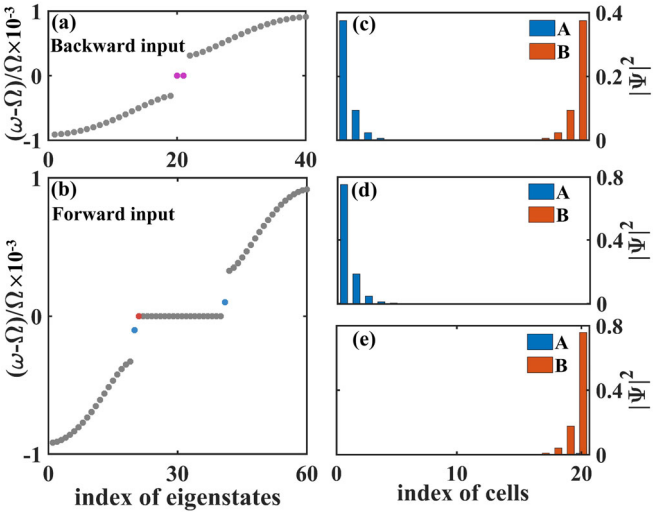

FIG. 3. Nonreciprocal energy spectra (a),(b) and probability distribution (c)–(e). (a) and (c) for the $\mathrm{CCW_A} - \mathrm{CW_B}$ supermode without coupling to the QEs, $g = 0$. (b), (d), and (e) for the $\mathrm{CW_A} - \mathrm{CCW_B}$ supermode with coupling to the QEs, $g/\Omega = 10^{-4}$. Other parameters are $J_1/\Omega = 3 \times 10^{-4}$, $J_2 = 2J_1$.

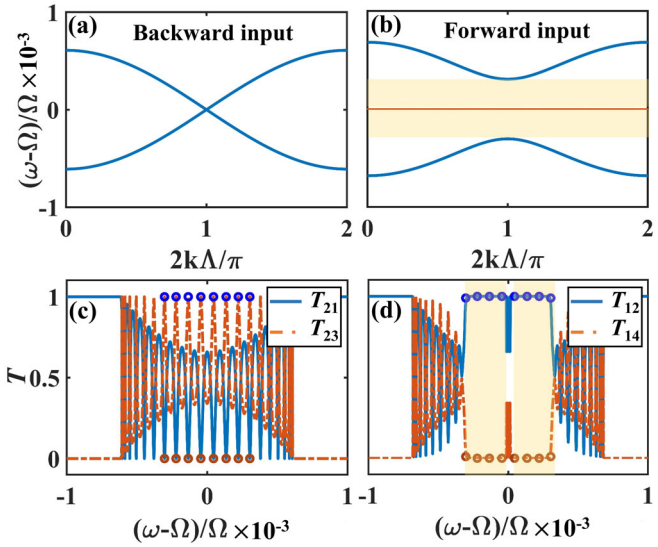

FIG. 4. Single-photon band structure (a),(b) and transmission (c),(d) with $N = 10$ for $J_1 = J_2$. In (a),(c) the $\mathrm{CCW_A} - \mathrm{CW_B}$ supermode is excited, and $g = 0$. In (b),(d) the $\mathrm{CW_A} - \mathrm{CCW_B}$ supermode is driven, and $g/\Omega = 3 \times 10^{-4}$. Other parameters are $J_1/\Omega = 3 \times 10^{-4}$, $J_2 = J_1$, and $\kappa_{\mathrm{in}} = \kappa_{\mathrm{out}} = 0.25i$.

from the QEs, equivalent to the conventional CROW without QEs. There are $2N$ peaks in the transmission T_{23} and dips in T_{21}. In contrast, when the single-photon wave packet inputs to port 1, the transmission T_{14} is zero because the photon transport is forbidden in the band gap, and thus $T_{12} = 1$; see Fig. 4(d). Clearly, we obtain strong nonreciprocity in the transmission at the frequencies corresponding to the peaks of T_{23}, where $T_{23} \approx 1$, or the dips of T_{21}, where $T_{21} \approx 0$. For $g/\Omega = 3 \times 10^{-4}$, we have eight nonreciprocal frequency windows at $(\omega - \Omega)/\Omega \approx \{\pm 30, \pm 22, \pm 13, \pm 4.5\} \times 10^{-5}$; see the blue circles. Because of the symmetry of the CROW, we obtain $T_{12} = T_{34}$ and $T_{23} = T_{41}$. Thus, we can choose any one of eight frequencies in the band-gap region to achieve $T_{23} = 1$ ($T_{21} = 0$). In this case, we can attain a frequency-multiplexed single-photon circulator with a circling photon transport direction $1 \to 2 \to 3 \to 4 \to 1$ at frequencies marked by circles in Fig. 4(d).

Note that this single-photon circulator is robust against backscattering (see the Supplemental Material [64]). The chiral coupling between the QE and the vacuum field of R_A eigenmodes induces an extra phase shift $\mathrm{Re}[\varphi]$ for the CW mode, shifting its resonance frequency and leading to nondegenerate with the CCW mode. Thus, the opposite CW mode excited by a backscattering of a propagating CCW mode is forbidden in the nonreciprocal band gap; see Figs. 4(a) and 4(b). Our chiral QE-CROW system promises a new type of backscattering-immune optical device.

Implementation.—The required 1D CROW can be made with silicon oxynitride [79], silicon on insulator [80,81], or lithium niobium oxynitride [82]. We consider a QE-CROW system consisting of $N = 10$ resonators with a radius of $r = 40$ μm and $n_{\mathrm{eff}} = 2$, yielding $\mathcal{F}/2\pi = 0.6$ THz. The external dissipations of resonators can be calculated as $\gamma_{\mathrm{ex}}/2\pi = 19.4$ GHz (setting $\gamma_{\mathrm{in}} = 0.02\gamma_{\mathrm{ex}}$, thus $\gamma_{\mathrm{tol}}/2\pi = (\gamma_{\mathrm{ex}} + \gamma_{\mathrm{in}})/2\pi = 19.8$ GHz) [70]. We take $\Omega/2\pi = 195$ GHz, and the coupling strength between resonators $J_1/\gamma_{\mathrm{tol}} = J_2/\gamma_{\mathrm{tol}} = 3$. Regarding QEs, we choose $\lambda = 1.538$ μm [83–85] so that $\omega_q = \Omega$ and a dipole moment of $|\mathbf{d}| = 20$ Debye [86], yielding $\gamma = 2\pi \times 5.48$ MHz, and $g/\gamma_{\mathrm{tol}} = 0.77$ for a resonator mode volume of $V_{\mathrm{m}} = 2.0$ $\mu\mathrm{m}^3$ [36,87]. The chiral QE-light interaction can be optically induced as aforementioned. The fidelity and the average photon survival probability of the circulator are calculated as $\{0.99, 0.98\}$ at two optimal frequency windows $(\omega - \Omega)/\Omega \approx \pm 4.5 \times 10^{-5}$ [15,30]. Moreover, we achieve a nonreciprocal transmission bandwidth of $\sim 2\pi \times 2.4$ GHz and an average insertion loss of 1.12 dB for a circulator fidelity larger than 0.95. Our first-principle simulation using the finite-difference time-domain method gives the transmissions in good agreement with the results of the transfer matrix method [64].

Discussion and conclusion.—We note that quantum nonreciprocity has been previously realized in a chiral quantum optical system using a single resonator or an optical waveguide [29–31,33,34,36]. Nevertheless, this achievement so far requires the strong coupling regime and/or only demonstrates a single nonreciprocal window. We have shown that nonreciprocal single-photon band structures can be achieved in our chiral QE-CROW system. In contrast, our single-photon circulator works in the weak coupling regime, greatly relaxing its experimental challenge. It is backscattering-immune and allows multifrequency nonreciprocal channels at the same time. Our work extends photonic band structures of periodic photonic structures to exhibit remarkable magnetic-free quantum nonreciprocity, likely beyond condensed matter.

K. X. and Y. L. thank Professor Haiqing Lin for his stimulating and constructive discussion. J. T. thanks Chaohua Wu for helpful discussions. This work is supported by the National Key R&D Program of China (Grants No. 2019YFA0308700, No. 2017YFA0303703, and No. 2017YFA0303701), the National Natural Science Foundation of China (Grants No. 11874212, No. 11890704, No. 11690031, and No. 12105025), the Fundamental Research Funds for the Central Universities (Grant No. 021314380095), the Program for Innovative Talents and Teams in Jiangsu (Grant No. JSSCTD202138), and the Excellent Research Program of Nanjing University (Grant No. ZYJH002). F. N. is supported in part by Nippon Telegraph and Telephone Corporation (NTT) Research, the Japan Science and Technology Agency (JST) (via the Quantum Leap Flagship Program (Q-LEAP), and the Moonshot R&D Grant No. JPMJMS2061), the Japan Society for the Promotion of Science (JSPS) (via the Grants-in-Aid for Scientific Research (KAKENHI) Grant No. JP20H00134), the Army Research Office (ARO) (Grant No. W911NF-18-1-0358), the Asian Office of Aerospace Research and Development (AOARD) (via Grant No. FA2386-20-1-4069), and the Foundational Questions Institute Fund (FQXi) via Grant No. FQXi-IAF19-06. We thank the High Performance Computing Center of Nanjing University for allowing the numerical calculations on its blade cluster system.

*Corresponding author.
keyu.xia@nju.edu.cn

[1] A. B. Khanikaev and G. Shvets, Two-dimensional topological photonics, Nat. Photonics **11**, 763 (2017).
[2] T. Ozawa, H. M. Price, A. Amo, N. Goldman, M. Hafezi, L. Lu, M. C. Rechtsman, D. Schuster, J. Simon, O. Zilberberg, and I. Carusotto, Topological photonics, Rev. Mod. Phys. **91**, 015006 (2019).
[3] M. Bello, G. Platero, J. I. Cirac, and A. González-Tudela, Unconventional quantum optics in topological waveguide QED, Sci. Adv. **5**, eaaw0297 (2019).
[4] X. Xi, J. Ma, S. Wan, C.-H. Dong, and X. Sun, Observation of chiral edge states in gapped nanomechanical graphene, Sci. Adv. **7**, eabe1398 (2021).

[5] H. J. Kimble, The quantum internet, Nature (London) **453**, 1023 (2008).
[6] Y.-P. Wang, J. W. Rao, Y. Yang, P.-C. Xu, Y. S. Gui, B. M. Yao, J. Q. You, and C.-M. Hu, Nonreciprocity and Unidirectional Invisibility in Cavity Magnonics, Phys. Rev. Lett. **123**, 127202 (2019).
[7] M. Liu, C. Zhao, Y. Zeng, Y. Chen, C. Zhao, and C.-W. Qiu, Evolution and Nonreciprocity of Loss-Induced Topological Phase Singularity Pairs, Phys. Rev. Lett. **127**, 266101 (2021).
[8] Y.-l. Ren, S.-l. Ma, J.-k. Xie, X.-k. Li, M.-t. Cao, and F.-l. Li, Nonreciprocal single-photon quantum router, Phys. Rev. A **105**, 013711 (2022).
[9] Ş. K. Özdemir, S. Rotter, F. Nori, and L. Yang, Parity-time symmetry and exceptional points in photonics, Nat. Mater. **18**, 783 (2019).
[10] D. Jalas, A. Petrov, M. Eich, W. Freude, S. Fan, Z. Yu, R. Baets, M. Popović, A. Melloni, J. D. Joannopoulos, M. Vanwolleghem, C. R. Doerr, and H. Renner, What is—and what is not—an optical isolator, Nat. Photonics **7**, 579 (2013).
[11] Y. Jiang, S. Maayani, T. Carmon, F. Nori, and H. Jing, Nonreciprocal phonon laser, Phys. Rev. Applied **10**, 064037 (2018).
[12] B. Peng, Ş. K. Özdemir, F. Lei, F. Monifi, M. Gianfreda, G. L. Long, S. Fan, F. Nori, C. M. Bender, and L. Yang, Parity-time-symmetric whispering-gallery microcavities, Nat. Phys. **10**, 394 (2014).
[13] Q.-T. Cao, H. Wang, C.-H. Dong, H. Jing, R.-S. Liu, X. Chen, L. Ge, Q. Gong, and Y.-F. Xiao, Experimental Demonstration of Spontaneous Chirality in a Nonlinear Microresonator, Phys. Rev. Lett. **118**, 033901 (2017).
[14] S. Zhang, Y. Hu, G. Lin, Y. Niu, K. Xia, J. Gong, and S. Gong, Thermal-motion-induced non-reciprocal quantum optical system, Nat. Photonics **12**, 744 (2018).
[15] K. Xia, F. Nori, and M. Xiao, Cavity-Free Optical Isolators and Circulators Using a Chiral Cross-Kerr Nonlinearity, Phys. Rev. Lett. **121**, 203602 (2018).
[16] P. Yang, X. Xia, H. He, S. Li, X. Han, P. Zhang, G. Li, P. Zhang, J. Xu, Y. Yang, and T. Zhang, Realization of Nonlinear Optical Nonreciprocity on a Few-Photon Level Based on Atoms Strongly Coupled to an Asymmetric Cavity, Phys. Rev. Lett. **123**, 233604 (2019).
[17] E.-Z. Li, D.-S. Ding, Y.-C. Yu, M.-X. Dong, L. Zeng, W.-H. Zhang, Y.-H. Ye, H.-Z. Wu, Z.-H. Zhu, W. Gao, G.-C. Guo, and B.-S. Shi, Experimental demonstration of cavity-free optical isolators and optical circulators, Phys. Rev. Research **2**, 033517 (2020).
[18] L. Tang, J. Tang, H. Wu, J. Zhang, M. Xiao, and K. Xia, Broad-intensity-range optical nonreciprocity based on feedback-induced Kerr nonlinearity, Photonics Res. **9**, 1218 (2021).
[19] L. Tang, J. Tang, M. Chen, F. Nori, M. Xiao, and K. Xia, Quantum Squeezing Induced Optical Nonreciprocity, Phys. Rev. Lett. **128**, 083604 (2022).
[20] M. Hafezi and P. Rabl, Optomechanically induced non-reciprocity in microring resonators, Opt. Express **20**, 7672 (2012).
[21] Z. Shen, Y.-L. Zhang, Y. Chen, C.-L. Zou, Y.-F. Xiao, X.-B. Zou, F.-W. Sun, G.-C. Guo, and C.-H. Dong, Experimental realization of optomechanically induced non-reciprocity, Nat. Photonics **10**, 657 (2016).
[22] F. Ruesink, M.-A. Miri, A. Alù, and E. Verhagen, Nonreciprocity and magnetic-free isolation based on optomechanical interactions, Nat. Commun. **7**, 13662 (2016).
[23] S. Maayani, R. Dahan, Y. Kligerman, E. Moses, A. U. Hassan, H. Jing, F. Nori, D. N. Christodoulides, and T. Carmon, Flying couplers above spinning resonators generate irreversible refraction, Nature (London) **558**, 569 (2018).
[24] R. Huang, A. Miranowicz, J.-Q. Liao, F. Nori, and H. Jing, Nonreciprocal Photon Blockade, Phys. Rev. Lett. **121**, 153601 (2018).
[25] D.-W. Wang, H.-T. Zhou, M.-J. Guo, J.-X. Zhang, J. Evers, and S.-Y. Zhu, Optical Diode Made from a Moving Photonic Crystal, Phys. Rev. Lett. **110**, 093901 (2013).
[26] S. A. R. Horsley, J.-H. Wu, M. Artoni, and G. C. La Rocca, Optical Nonreciprocity of Cold Atom Bragg Mirrors in Motion, Phys. Rev. Lett. **110**, 223602 (2013).
[27] D. L. Sounas and A. Alù, Non-reciprocal photonics based on time modulation, Nat. Photonics **11**, 774 (2017).
[28] C. Sayrin, C. Junge, R. Mitsch, B. Albrecht, D. O'Shea, P. Schneeweiss, J. Volz, and A. Rauschenbeutel, Nanophotonic Optical Isolator Controlled by the Internal State of Cold Atoms, Phys. Rev. X **5**, 041036 (2015).
[29] K. Xia, G. Lu, G. Lin, Y. Cheng, Y. Niu, S. Gong, and J. Twamley, Reversible nonmagnetic single-photon isolation using unbalanced quantum coupling, Phys. Rev. A **90**, 043802 (2014).
[30] M. Scheucher, A. Hilico, E. Will, J. Volz, and A. Rauschenbeutel, Quantum optical circulator controlled by a single chirally coupled atom, Science **354**, 1577 (2016).
[31] P. Lodahl, S. Mahmoodian, S. Stobbe, A. Rauschenbeutel, P. Schneeweiss, J. Volz, H. Pichler, and P. Zoller, Chiral quantum optics, Nature (London) **541**, 473 (2017).
[32] M. J. Mehranad, A. P. Foster, R. Dost, E. Clarke, P. K. Patil, A. M. Fox, M. S. Skolnick, and L. R. Wilson, Chiral topological photonics with an embedded quantum emitter, Optica **7**, 1690 (2020).
[33] M.-X. Dong, K. Xia, W.-H. Zhang, Y.-C. Yu, Y.-H. Ye, E.-Z. Li, L. Zeng, D.-S. Ding, B.-S. Shi, G.-C. Guo, and F. Nori, All-optical reversible single-photon isolation at room temperature, Sci. Adv. **7**, eabe8924 (2021).
[34] X.-X. Hu, Z.-B. Wang, P. Zhang, G.-J. Chen, Y.-L. Zhang, G. Li, X.-B. Zou, T. Zhang, H. X. Tang, C.-H. Dong, G.-C. Guo, and C.-L. Zou, Noiseless photonic non-reciprocity via optically-induced magnetization, Nat. Commun. **12**, 2389 (2021).
[35] S. Pucher, C. Liedl, S. Jin, A. Rauschenbeutel, and P. Schneeweiss, Atomic spin-controlled non-reciprocal Raman amplification of fibre-guided light, arXiv:2107.07272.
[36] L. Tang, J. Tang, W. Zhang, G. Lu, H. Zhang, Y. Zhang, K. Xia, and M. Xiao, On-chip chiral single-photon interface: Isolation and unidirectional emission, Phys. Rev. A **99**, 043833 (2019).
[37] T. Ramos, H. Pichler, A. J. Daley, and P. Zoller, Quantum Spin Dimers from Chiral Dissipation in Cold-Atom Chains, Phys. Rev. Lett. **113**, 237203 (2014).
[38] I. Söllner, S. Mahmoodian, S. L. Hansen, L. Midolo, A. Javadi, G. Kiršanskė, T. Pregnolato, H. El-Ella, E. H. Lee, J. D. Song, S. Stobbe, and P. Lodahl, Deterministic

photon-emitter coupling in chiral photonic circuits, Nat. Nanotechnol. **10**, 775 (2015).
[39] T. Li, Z. Gao, and K. Xia, Nonlinear-dissipation-induced nonreciprocal exceptional points, Opt. Express **29**, 17613 (2021).
[40] J. Tang, L. Tang, H. Wu, Y. Wu, H. Sun, H. Zhang, T. Li, Y. Lu, M. Xiao, and K. Xia, Towards On-Demand Heralded Single-Photon Sources via Photon Blockade, Phys. Rev. Applied **15**, 064020 (2021).
[41] D. Roy, C. M. Wilson, and O. Firstenberg, Colloquium: Strongly interacting photons in one-dimensional continuum, Rev. Mod. Phys. **89**, 021001 (2017).
[42] D. E. Chang, J. S. Douglas, A. González-Tudela, C.-L. Hung, and H. J. Kimble, Colloquium: Quantum matter built from nanoscopic lattices of atoms and photons, Rev. Mod. Phys. **90**, 031002 (2018).
[43] A. Yariv, Y. Xu, R. K. Lee, and A. Scherer, Coupled-resonator optical waveguide: A proposal and analysis, Opt. Lett. **24**, 711 (1999).
[44] J. K. S. Poon, J. Scheuer, S. Mookherjea, G. T. Paloczi, Y. Huang, and A. Yariv, Matrix analysis of microring coupled-resonator optical waveguides, Opt. Express **12**, 90 (2004).
[45] J. Perczel, J. Borregaard, D. E. Chang, S. F. Yelin, and M. D. Lukin, Topological Quantum Optics Using Atomlike Emitter Arrays Coupled to Photonic Crystals, Phys. Rev. Lett. **124**, 083603 (2020).
[46] Y. Ao, X. Hu, Y. You, C. Lu, Y. Fu, X. Wang, and Q. Gong, Topological Phase Transition in the Non-Hermitian Coupled Resonator Array, Phys. Rev. Lett. **125**, 013902 (2020).
[47] J. Li, B. Gao, C. Zhu, J. Xu, and Y. Yang, Nonreciprocal photonic composited Su-Schrieffer-Heeger chain, Appl. Phys. Lett. **119**, 141108 (2021).
[48] E. Kim, X. Zhang, V. S. Ferreira, J. Banker, J. K. Iverson, A. Sipahigil, M. Bello, A. González-Tudela, M. Mirhosseini, and O. Painter, Quantum Electrodynamics in a Topological Waveguide, Phys. Rev. X **11**, 011015 (2021).
[49] D. De Bernardis, Z.-P. Cian, I. Carusotto, M. Hafezi, and P. Rabl, Light-Matter Interactions in Synthetic Magnetic Fields: Landau-Photon Polaritons, Phys. Rev. Lett. **126**, 103603 (2021).
[50] J. C. Owens, M. G. Panetta, B. Saxberg, G. Roberts, S. Chakram, R. Ma, A. Vrajitoarea, J. Simon, and D. Schuster, Chiral cavity quantum electrodynamics, arXiv:2109.06033.
[51] K. Y. Bliokh and F. Nori, Characterizing optical chirality, Phys. Rev. A **83**, 021803(R) (2011).
[52] K. Y. Bliokh, D. Smirnova, and F. Nori, Quantum spin Hall effect of light, Science **348**, 1448 (2015).
[53] F. Alpeggiani, K. Y. Bliokh, F. Nori, and L. Kuipers, Electromagnetic Helicity in Complex Media, Phys. Rev. Lett. **120**, 243605 (2018).
[54] J. D. Thompson, T. G. Tiecke, N. P. de Leon, J. Feist, A. V. Akimov, M. Gullans, A. S. Zibrov, V. Vuletić, and M. D. Lukin, Coupling a single trapped atom to a nanoscale optical cavity, Science **340**, 1202 (2013).
[55] S. Barik, A. Karasahin, C. Flower, T. Cai, H. Miyake, W. DeGottardi, M. Hafezi, and E. Waks, A topological quantum optics interface, Science **359**, 666 (2018).
[56] J. Yang *et al.*, Diabolical points in coupled active cavities with quantum emitters, Light Sci. Appl. **9**, 6 (2020).
[57] S. Guddala, Y. Kawaguchi, F. Komissarenko, S. Kiriushechkina, A. Vakulenko, K. Chen, A. Alù, V. M. Menon, and A. B. Khanikaev, All-optical nonreciprocity due to valley polarization pumping in transition metal dichalcogenides, Nat. Commun. **12**, 3746 (2021).
[58] R. Shreiner, K. Hao, A. Butcher, and A. A. High, Electrically controllable chirality in a nanophotonic interface with a two-dimensional semiconductor, Nat. Photonics **16**, 330 (2022).
[59] A. Branny, S. Kumar, R. Proux, and B. D. Gerardot, Deterministic strain-induced arrays of quantum emitters in a two-dimensional semiconductor, Nat. Commun. **8**, 15053 (2017).
[60] C. Palacios-Berraquero, D. M. Kara, A. R. P. Montblanch, M. Barbone, P. Latawiec, D. Yoon, A. K. Ott, M. Loncar, A. C. Ferrari, and M. Atatüre, Large-scale quantum-emitter arrays in atomically thin semiconductors, Nat. Commun. **8**, 15093 (2017).
[61] M. Biondi, E. P. L. van Nieuwenburg, G. Blatter, S. D. Huber, and S. Schmidt, Incompressible Polaritons in a Flat Band, Phys. Rev. Lett. **115**, 143601 (2015).
[62] W. P. Su, J. R. Schrieffer, and A. J. Heeger, Solitons in Polyacetylene, Phys. Rev. Lett. **42**, 1698 (1979).
[63] Z.-Q. Jiao, S. Longhi, X.-W. Wang, J. Gao, W.-H. Zhou, Y. Wang, Y.-X. Fu, L. Wang, R.-J. Ren, L.-F. Qiao, and X.-M. Jin, Experimentally Detecting Quantized Zak Phases without Chiral Symmetry in Photonic Lattices, Phys. Rev. Lett. **127**, 147401 (2021).
[64] See Supplemental Material at http://link.aps.org/supplemental/10.1103/PhysRevLett.128.203602 for the detailed derivations of our main results, which includes Refs. [65–69].
[65] Y. Peng, Y. Bao, and F. von Oppen, Boundary Green functions of topological insulators and superconductors, Phys. Rev. B **95**, 235143 (2017).
[66] M. Hafezi, E. A. Demler, M. D. Lukin, and J. M. Taylor, Robust optical delay lines with topological protection, Nat. Phys. **7**, 907 (2011).
[67] M. Scollon and M. P. Kennett, Persistence of chirality in the Su-Schrieffer-Heeger model in the presence of on-site disorder, Phys. Rev. B **101**, 144204 (2020).
[68] D. F. Walls and G. J. Milburn, *Quantum Optics*, 2nd ed. (Springer Science & Business Media, Berlin, Germany, 2007).
[69] J.-T. Shen and S. Fan, Theory of single-photon transport in a single-mode waveguide. I. Coupling to a cavity containing a two-level atom, Phys. Rev. A **79**, 023837 (2009).
[70] J.-S. Tang, L. Tang, and K. Xia, Three methods for the single-photon transport in a chiral cavity quantum electrodynamics system, Chin. Opt. Lett. **20**, 062701 (2022).
[71] J. K. Asbóth, L. Oroszlány, and A. Pályi, A short course on topological insulators: Band-structure and edge states in one and two dimensions, Lect. Notes Phys. **919**, 166 (2016).
[72] M. F. Yanik, W. Suh, Z. Wang, and S. Fan, Stopping Light in a Waveguide with an All-Optical Analog of Electromagnetically Induced Transparency, Phys. Rev. Lett. **93**, 233903 (2004).
[73] P. Wang, Y. Zheng, X. Chen, C. Huang, Y. V. Kartashov, L. Torner, V. V. Konotop, and F. Ye, Localization and

delocalization of light in photonic moiré lattices, Nature (London) **577**, 42 (2020).
[74] Y. He, R. Mao, H. Cai, J.-X. Zhang, Y. Li, L. Yuan, S.-Y. Zhu, and D.-W. Wang, Flat-Band Localization in Creutz Superradiance Lattices, Phys. Rev. Lett. **126**, 103601 (2021).
[75] V. M. Martinez Alvarez and M. D. Coutinho-Filho, Edge states in trimer lattices, Phys. Rev. A **99**, 013833 (2019).
[76] M. Kremer, I. Petrides, E. Meyer, M. Heinrich, O. Zilberberg, and A. Szameit, A square-root topological insulator with non-quantized indices realized with photonic Aharonov-Bohm cages, Nat. Commun. **11**, 907 (2020).
[77] G. Cáceres-Aravena, B. Real, D. Guzmán-Silva, A. Amo, L. E. F. Foa Torres, and R. A. Vicencio, Experimental observation of edge states in SSH-Stub photonic lattices, Phys. Rev. Research **4**, 013185 (2022).
[78] A. Anastasiadis, G. Styliaris, R. Chaunsali, G. Theocharis, and F. K. Diakonos, Bulk-edge correspondence in the trimer Su-Schrieffer-Heeger model, arXiv:2202.13789.
[79] C. F. Andrea Melloni, Francesco Morichetti, and M. Martinelli, Continuously tunable 1 byte delay in coupled-resonator optical waveguides, Opt. Lett. **33**, 2389 (2008).
[80] M. Hafezi, S. Mittal, J. Fan, A. Migdall, and J. M. Taylor, Imaging topological edge states in silicon photonics, Nat. Photonics **7**, 1001 (2013).
[81] J. Wang, Z. Yao, and A. W. Poon, Silicon-nitride-based integrated optofluidic biochemical sensors using a coupled-resonator optical waveguide, Front. Mater. **2**, 1 (2015).
[82] M. Wang, N. Yao, R. Wu, Z. Fang, S. Lv, J. Zhang, J. Lin, W. Fang, and Y. Cheng, Strong nonlinear optics in on-chip coupled lithium niobate microdisk photonic molecules, New J. Phys. **22**, 073030 (2020).
[83] A. Kors, J. P. Reithmaier, and M. Benyoucef, Telecom wavelength single quantum dots with very small excitonic fine-structure splitting, Appl. Phys. Lett. **112**, 172102 (2018).
[84] S. Haffouz, K. D. Zeuner, D. Dalacu, P. J. Poole, J. Lapointe, D. Poitras, K. Mnaymneh, X. Wu, M. Couillard, M. Korkusinski, E. Schöll, K. D. Jöns, V. Zwiller, and R. L. Williams, Bright single inasp quantum dots at telecom wavelengths in position-controlled inp nanowires: The role of the photonic waveguide, Nano Lett. **18**, 3047 (2018).
[85] Y. Arakawa and M. J. Holmes, Progress in quantum-dot single photon sources for quantum information technologies: A broad spectrum overview, Appl. Phys. Rev. **7**, 021309 (2020).
[86] H. Htoon, T. Takagahara, D. Kulik, O. Baklenov, A. L. Holmes, and C. K. Shih, Interplay of Rabi Oscillations and Quantum Interference in Semiconductor Quantum Dots, Phys. Rev. Lett. **88**, 087401 (2002).
[87] Q. Xu, D. Fattal, and R. G. Beausoleil, Silicon microring resonators with 1.5-μm radius, Opt. Express **16**, 4309 (2008).